



Design of structural coloration for full-color high-definition computer-generated holograms

SANGWON HAM,¹ SUNGJAE PARK,² SEONG WOO JANG,¹
JONGHYUN LEE,²  BYEONG-KWON JU,^{1,3}  AND HWI KIM^{2,4} 

¹Display and Nanosystem Laboratory, College of Engineering, Korea University, Seoul, 136-713, Republic of Korea

²Department of Electronics and Information Engineering, Korea University, Sejong Campus 2511 Sejong-ro 30019, Republic of Korea

³bkju@korea.ac.kr

⁴hwikim@korea.ac.kr

Abstract: This paper investigates the submicron scale color filter design in the high-definition computer-generated hologram (HD-CGH). It is addressed that single pixel structural coloration is essential for full-color wide-viewing angle HD-CGH because the conventional RGB color stripe filter degrades HD-CGH image quality due to low misalignment tolerance. Considering that a submicron scale slit or hole with metallic mirror sidewalls can operate as a single pixel color filter. We propose a design of single pixel RGB plasmonic color filter (PCF) and present the feasibility of applying the proposed single pixel RGB PCF to high-definition HD-CGHs. Based on the RGB PCF platform, a $1.1 \mu\text{m} \times 1.1 \mu\text{m}$ RGB PCF is designed and the corresponding optical characteristics of the full-color HD-CGH are analyzed.

© 2022 Optica Publishing Group under the terms of the [Optica Open Access Publishing Agreement](#)

1. Introduction

The plasmonic color filter (PCF) is a promising platform for replacing conventional pigment-based polymer absorptive color filters [1–4]. Research on various methods of realizing structural color filters are in progress and one of the central concepts is controlling the resonance coupling of photons to plasmonic cavities in order to enable filtering light of the desired wavelength band. Efficient and miniaturized pixel technology at the micron-scale has been researched to realize high-resolution displays including sub-wavelength scale PCF [5,6]. PCFs have been studied in various shape arrays such as planar multilayers, gratings, and periodic hole patterns [7–14]. The resonance wavelengths of PCFs with high transmission or reflectivity in the visible wavelength band are determined by the factors associated with materials and geometries. [15–20].

Compared to pigment-based color filters, PCFs maintain their color characteristics under the sub-micro scale, and this is largely why PCFs have been attracting substantial interest as a unique color filter platform for the visible wavelength band [21–24]. Conventionally, the long-range effect induced by periodicity has been considered essential for structural color filter mechanisms [25]. However, recent applications require sub-micro scale single pixel color filters, for which the long-range effect based on structural periodicity needs to be overcome because such periodicity cannot satisfy the sub-micro dimensional specification.

In the recently proposed mirrored color filter structure [26–28], the periodic boundary condition allows an effective periodicity that provokes the transmissive PCF effect. It seems that the mirror sidewall not only makes a lateral cavity structure but also acts a shelter from optical crosstalk by isolating adjacent mirrored filters. A normal metallic mirror sidewall over 50 nm thick can generate a mirrored color filter, and within the volume of the mirrored color filter, several plasmonic modes such as plasmonic gap mode, surface plasmonic mode, and lateral Fabry-Pérot mode are induced. Theoretically, the performance of color filters such as transmission efficiency and full width at half maximum (FWHM) can be greatly improved if multiple modes are excited

simultaneously [29]. In practice, enhancing both transmission efficiency and color purity are key issues for the mirrored color filter structure. Furthermore, the possibility of the active tuning of mirrored color filters raises strong research interest because a single tiny volume is more effectively controllable than spatially extended periodic structures via electro-optic effects or phase-change mechanisms.

The high-definition computer-generated hologram (HD-CGH) is a large-scale CGH reconstructing a wide-viewing angle three-dimensional (3D) scene [30]. The wide-viewing angle of the HD-CGH is enabled by the wavelength scale submicron pixel size. The coloring of HD-CGHs, although an important issue, is a relatively new research topic. Expressing all the colors within the unit pixel of a HD-CGH is preferable, but realizing this at fabrication stage is challenging.

Recently, a full color HD-CGH featuring a color filter layer of basic RGB stripe patterns has been reported [31–34]. Full-color high-definition computer-generated holograms can be obtained by attaching a RGB stripe-pattern color filter wider than a single pixel pitch to the CGH plate, unfortunately leading to image quality degradation. When the width of the RGB stripe-pattern color filter is comparable to the single pixel pitch, the misalignment between the CGH pattern and the color filter layer can lead to significant color degradation or wrong coloration. The vertical detachment of the CGH pattern and the color filter layer may cause the relative lateral shift according to the viewer's position. The numerical simulation will present that the color of the HD-CGH varies significantly according to the viewer's position. Therefore, the best design of full-color HD-CGH is the in-plane color HD-CGH with modulation pixels merged with RGB color filters, i.e. color-pixel HD-CGH. We have thought that the best approach for color-pixel HD-CGHs is utilizing RGB PCF composite.

In this paper, we manifest the coloration issue of HD-CGHs associated with misalignment induced color crosstalk and propose a PCF based color-pixel HD-CGH design to solve the problem. The optical characteristics of the PCF based single pixel and the HD-CGH image quality is investigated in terms of color variation according to the viewing angle. Ultimately, we will show that the PCF single pixel enables full-color HD-CGHs featuring wide-viewing angle color stabilization.

2. Coloration of high-definition computer-generated hologram

The coloration of high-definition CGHs has been accomplished by stripe-type color filter layers, as shown in Fig. 1(a). Figure 1 compares the distinctive approaches of HD-CGH coloration using the conventional stripe color filter layer above the CGH plane and the in-plane color pixel HD-CGH, which combines the color filter and HD-CGH pixel (Fig. 1(b)).

The issue of the conventional layered structure is its low angular color tolerance. The HD-CGH color image quality can be deteriorated by angular misalignment of the color filter layer and the CGH plate, and the inter diffraction crosstalk induced by the strong diffraction of the CGH pixel in the intermediate gap between the CGH plate and the color filter. For obliquely incident waves, the CGH and color filter plate becomes spatially mismatched. The viewer can then observe color-crosstalk due to gap diffraction. It is intuitively apparent that a conventional layered structure with a vertical gap is vulnerable to color inversion and color crosstalk or color blurring.

Let the width of the color stripe and the HD-CGH pixel pitch be denoted by W and p . The extreme case of $W = p$ is not practical when the gap distance between the CGH plate and the color filter plane is greater than p . A numerical wave optic simulation [30] shows that, as shown in Fig. 1(a), when using the layered stripe color-filter structure, observing HD-CGH from an off-axis position or with incident light (lower panel) may cause confusion in the color expression of a cube image with a red front, blue side, and green top. On the other hand, in the unified color-pixel HD-CGH, accurate color expression can be confirmed in all observation area, as presented in Fig. 1(b).

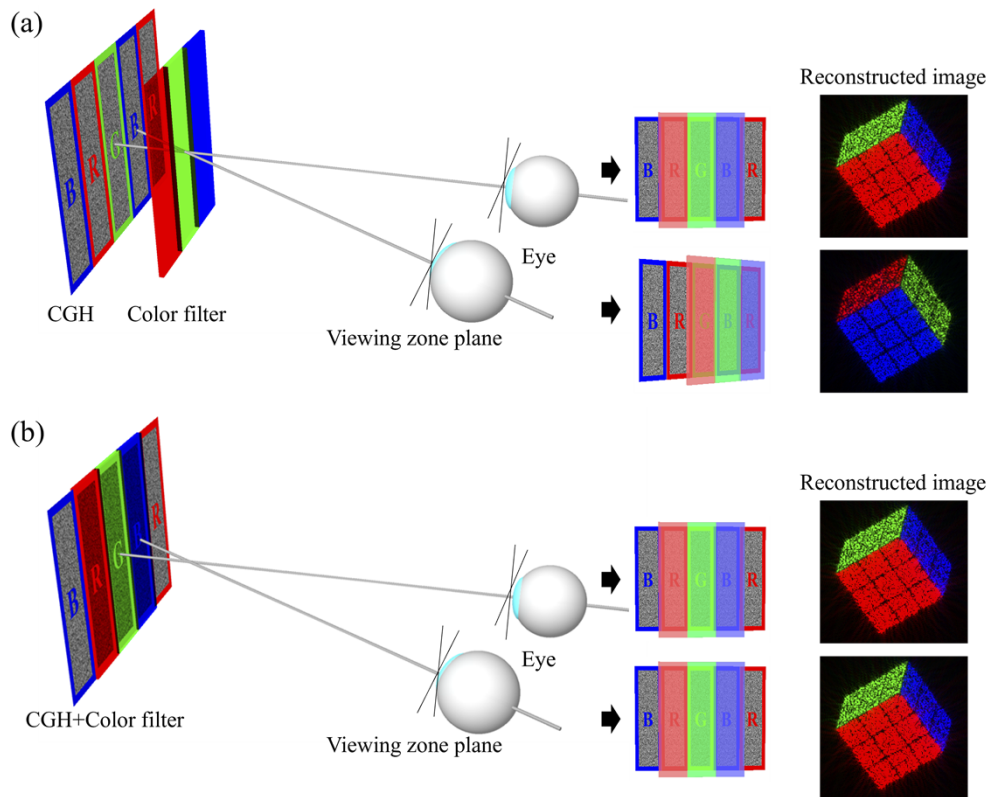


Fig. 1. HD-CGH coloration scheme. (a) Layered stripe color filter structure, and (b) unified color-pixel structure. The layered stripe color filter structure is sensitive to the viewing angle, while the unified color pixel structure conserves colors stably.

The stripe color pattern narrows the viewing zone horizontally or vertically along the direction orthogonal to the stripe line width. Figure 2 presents the definition of the basic mask arrangement, and shows the resulting characteristics in the viewing zone plane (Fourier domain). To understand the effect of the RGB masks, we simulated a single field of view of a complex-valued CGH, as presented in Fig. 2(a). If a vertical stripe mask is used, the signal data is replicated horizontally in the viewing zone plane (Fig. 2(b)).

Conversely, if a horizontally aligned mask array is used, the signal data is replicated vertically (Fig. 2(c)). Furthermore, it can be seen that as the width of the stripe color filter increases to $W = 2p$, the number of signal data duplications increases and the viewing angle narrows. Thus, the unification of color filter and CGH pattern at the single pixel level is desirable for the widest viewing angle and robust coloration.

Using our previously developed design method [30], a full-color wide viewing angle HD-CGH was calculated and a cube-shaped 3D object was reconstructed from various angles (center, top, bottom, left, right) in Fig. 3(a). Note that if the stripe pattern color filter is 1 pixel ($W = p$), only 1/3 of the total viewing area is used when calculating the HD-CGH. For the calculated HD-CGH, Fig. 3(b) shows the results of applying a stripe pattern color filter structure of a width of $W = p, 3p, 5p$ in the horizontal direction. A color filter mask size of 1 pixel (1p) is fine, but above 2 pixels (3p and 5p), the signal is duplicated and reconstructed images overlap. This phenomenon is expected from the signal duplication shown in the viewing zone field distribution of Figs. 2(b) and 2(c).

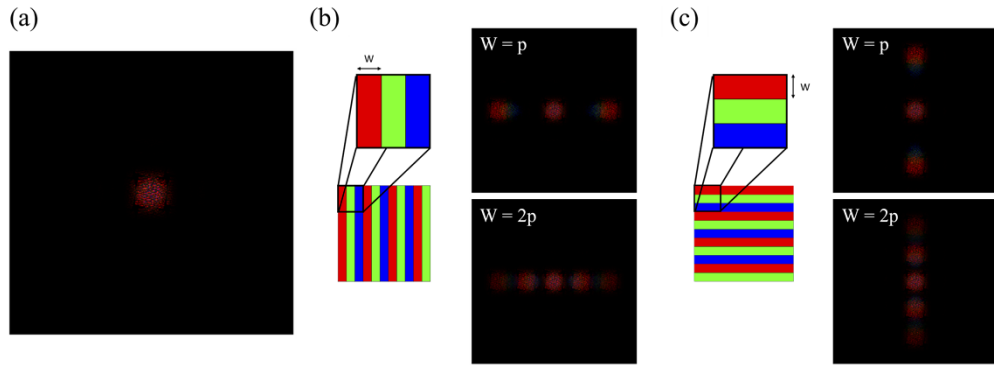


Fig. 2. (a) Single field of view in Fourier domain. (b) Vertical, (c) Horizontal striped mask and field distribution by mask size.

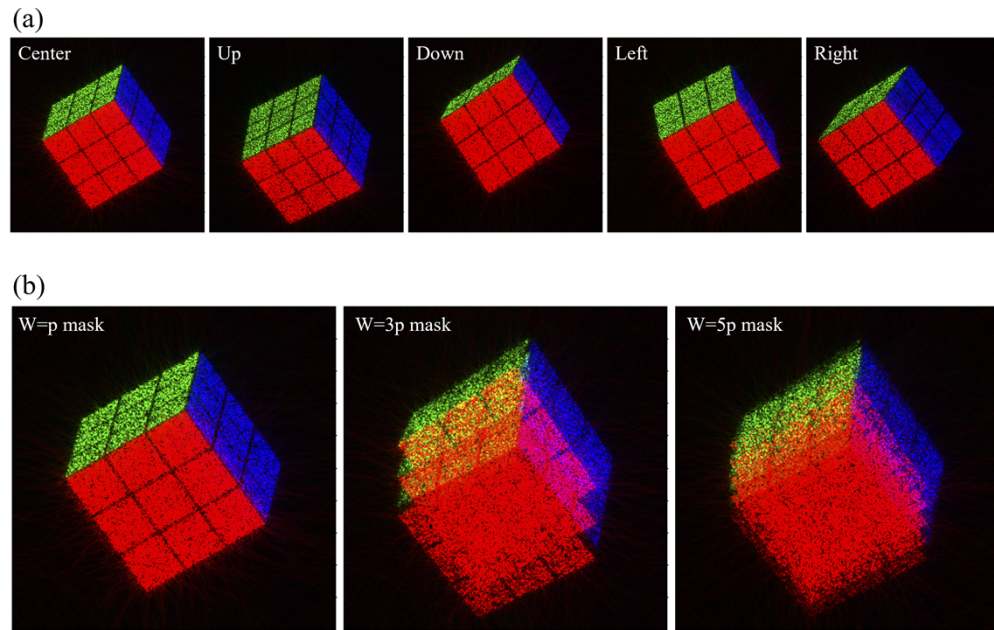


Fig. 3. (a) Reconstructed images from various angles (center, up, down, left, right) of full-color wide viewing angle HD-CGH. (b) Reconstructed images for stripe pattern color filter structures at $w = 1, 3, 5$ in the horizontal direction.

Our proposed PCF color pixel design may overcome this issue. In the following section, the RGB PCF color pixel compatible to HD-CGH is presented and its optical characteristics are discussed in terms of HD-CGH image quality and color tolerance.

3. Full-color PCF HD-CGH

The proposed design for full-color PCF HD-CGHs based on the single pixel PCF is presented in Fig. 4. By merging the CGH and color filter, we can prevent the misalignment-induced color distortion and crosstalk caused by the diffraction of CGH pixels. The design for full-color HD-CGHs features highly compact RGB color composite pixels.

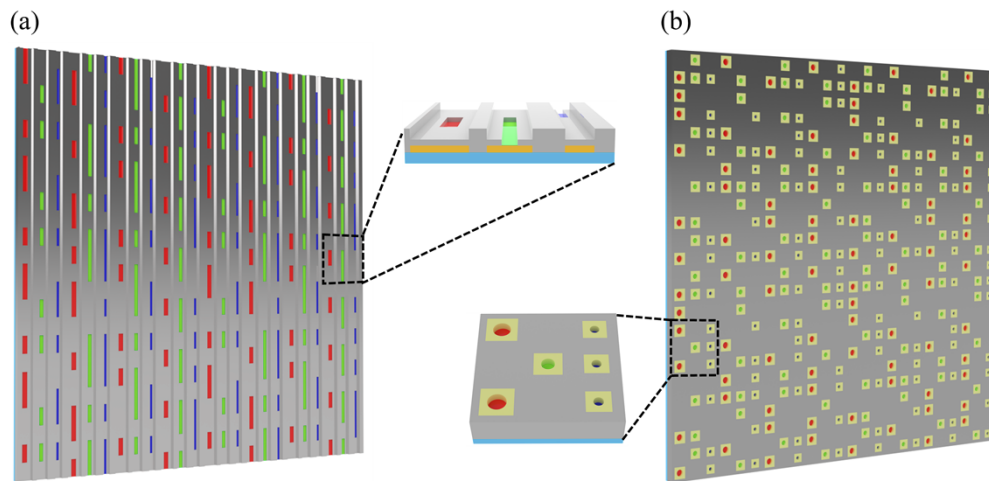


Fig. 4. Full-color PCF HD-CGH of (a) 1D single slit and (b) 2D single hole structure. (The enlarged area represents 3×3 size pixels of HD-CGH.)

As will be presented later, it is possible to design a submicron scale single pixel PCF to achieve a wide-viewing angle HD-CGH. As depicted in Figs. 4(a) and 4(b), 1D single slit and 2D hole HD-CGHs can be considered. For 465 nm wavelength (blue) light, a unit pixel size of $630 \text{ nm} \times 630 \text{ nm}$ produces a HD-CGH with a maximum viewing angle of 14.4° . Regarding the PCF color pixels, polarization as well as geometrical factors must be considered for clear color reproduction. The proposed 1D structure operates in TM mode, and the 2D hole pattern can operate in both TM and TE mode.

As depicted in Fig. 5, the PCF HD-CGH pixel is designed as single pixel PCFs with metallic mirror sidewall structures. Conceptually, the size of a single pixel PCF can be set equal to the period of the corresponding periodic array color filter, which means that a PCF single pixel can be isolated by the metallic mirror sidewalls. In this way, the metallic mirror sidewalls allow the embedded single unit to operate as the infinitely periodic array of the single unit. The geometric structures and materials used in the designs of the color filters are optimized to maximize the particular coloration effects.

As depicted in Figs. 5(a) and 5(d), the metallic mirror sidewalls of the 1D and 2D PCF pixels are erected in the z -axis direction. The unit cell structure of the periodic array color filter is modeled in the form of a single unit pixel of a submicron scale. In the field calculation and analysis of the optical properties, we employ the Fourier modal method (FMM) [35]. In order to suppress crosstalk occurring between adjacent unit pixels [26], we should analyze over an area sufficiently large to cover the distance between the red, green, and blue metallic mirror sidewalls.

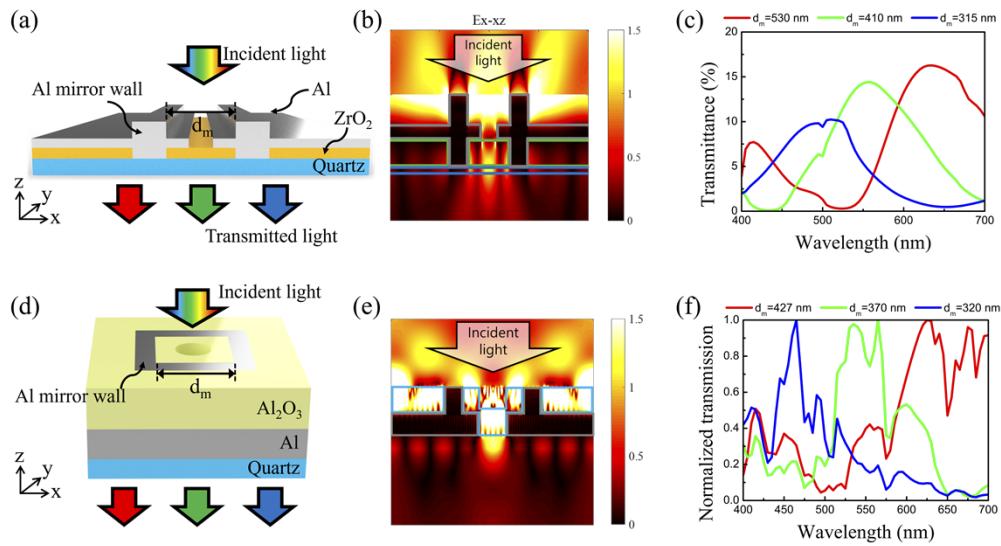


Fig. 5. Single pixel PCFs with metallic mirror sidewall. Schematic of (a) 1D, (d) 2D structure surrounded by metallic mirror sidewall around unit pixel. Electric field distribution profile in the x - z cross-section of (b) 1D, (e) 2D single pixel PCF. (Observed in the green color filter at 532 nm). Calculated transmission spectrum of the red, green and blue filters of (c) 1D and (f) 2D PCFs. (c) Transmittance spectrum of a 1D single pixel PCF with distances of 530 nm, 410 nm and 315 nm between metallic mirror sidewalls. Transmittance spectrum of a (f) 2D single pixel PCF with distances between metallic mirror sidewall of 427 nm, 370 nm and 320 nm.

The 1D single slit structure was simulated with a length of $2 \mu\text{m}$ along the x -axis, and the 2D hole structure was simulated with an area of $1 \mu\text{m} \times 1 \mu\text{m}$ in the x - y plane.

Before taking actual metal materials as mirror sidewalls in the numerical simulation, a calculation was made incorporating near perfect electric conducting (PEC) mirror sidewalls to check the operation of a single pixel color filter under the ideal mirror conditions. The PEC is set as a near perfect mirror, and the distance between the sidewalls corresponds to the same value as the period of the periodic array color filter structure, as shown in Appendix I (Fig. 8(a)). In Fig. 5, we replaced the PEC mirror sidewall with aluminum metal, reflecting a practical design approach, and then optimized the parameters of the structure through numerical simulation (Appendix II).

The designed 1D single pixel PCF consists of a 65 nm dielectric (ZrO_2) layer and a 55 nm metal (Al) grating on a quartz substrate. The distance between the metallic mirror sidewalls for the red, green and blue structure are 530 nm, 410 nm and 315 nm, respectively and the fill factor is 0.65 for all colors. The metallic mirror sidewalls are made of Al, and the height from the substrate surface is 200 nm. The only factor controlling the resonance wavelength is the distance between the metallic mirror sidewalls, the other parameters being the same. The 2D single pixel PCF consists of a 200 nm thick dielectric (Al_2O_3) layer and a 150 nm thick metal (Al) hole structure on a quartz substrate is presented. The distances between the metallic mirror sidewalls corresponding to red, green and blue are 420 nm, 370 nm, and 320 nm, respectively, and the hole diameters are 240 nm, 180 nm and 130 nm. The height of metallic mirror sidewalls is 200 nm, the same as the thickness of the Al_2O_3 layer.

The Fabry-Pérot interferometer has been completed by the placement of the metallic mirror sidewalls. A ZrO_2 layer is the medium layer inside the cavity in the Fabry-Pérot interferometer, and the metal sidewall acts as a mirror constituting the cavity. The resulting steady state field distribution is specified by the medium refractive index and the optical distance between the

mirror walls. As shown in Fig. 5(b), a standing wave generated by two fields propagating in opposite directions is observed in an electric field inside a single pixel color filter with metallic mirror sidewalls. Figure 5(c) shows the transmission spectrum of 1D red, green and blue single pixel PCF calculated under the TM polarization condition along the x-axis. The wavelength corresponding to the maximum transmittance is 635 nm for the red structure, 555 nm for the green structure, and 510 nm for the blue structure, and the corresponding transmittances are 16.3%, 14.4%, and 10.2%, respectively. The FWHMs of the red, green and blue structures are 136.38 nm, 128 nm and 116.1 nm, which are wider than the corresponding periodic color filter structures, but a high color gamut is expected because unnecessary secondary peaks do not occur.

In the field distribution of the 2D single pixel PCF presented in Fig. 5(e), field intensity enhancement is observed by the mirror sidewall surrounding the hole. Figure 5(f) presents the transmission spectrums of the 2D red, green and blue single pixel PCFs, and the resonance peak wavelengths of the 2D single hole color filters are observed at 625 nm, 565 nm and 465 nm, respectively, expressed as normalized transmission. The color filter characteristics of each color is manifested, but the low transmittance is a problem requiring further research.

For HD-CGH application, the coloration of PCF color pixels should be highly tolerable and robust to the incidence angle of light. The incident angle dependences of the single pixel PCF structure and the conventional periodic color filter are compared in Fig. 6. The single color pixel (right panel) is invariant in the transmission spectrum to the incidence angle variation from 0° to 20° , and has no second order resonance that is apparent in the periodic structure (left panel).

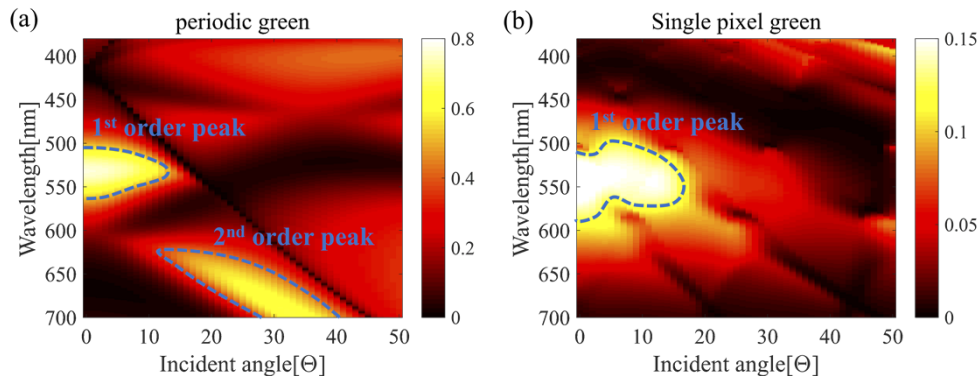


Fig. 6. Calculation comparing the transmission spectrum according to the range of the incident angle from 0° to 50° with the periodic structure in a single pixel PCF. (a) periodic green color filter. (b) single pixel green color filter.

The design of periodic array color filters, which is the basis structure for the design of single pixel PCF is further discussed in Appendix I. Comparing the single pixel PCF and the corresponding periodic PCF, we can see that the maximum transmittance in the single pixel PCF is observed when the distance between the metallic mirror sidewalls is reduced by 10 nm for red structure, 20 nm for green structure and 50 nm for blue structure. The resonant wavelength shifts when lengthening of the optical length in the x-axis direction because the electromagnetic field is reflected by penetrating the interface rather than by being directly reflected at the dielectric-metal interface [36–38]. Therefore, the structural tuning of the distance between the metal mirrors or the parameters of the metal mirrors can be optimized by compensating the related phase shift at the reflecting surfaces.

In Fig. 7, based on the single pixel PCF design method, the operation of the RGB composite pixel with integrated red, green and blue pixels was confirmed. For each red, green and blue PCF, the minimum metallic mirror side wall width that satisfies the penetration depth was chosen

to minimize the area of the integrated pixel and block inter-pixel crosstalk. The width of the adjacent metallic sidewall of each pixel is fixed at 100 nm, while the parameters specific to the red, green and blue 1D PCF structures remain the same as the design in Fig. 5(a). Overall, the total size of the pixel in the x-axis direction becomes 1.505 μm . In Fig. 7(a), the structure in which red, green and blue all operate shows that visible light is transmitted evenly across the entire visible light range, representing white color. This transmission of white light means that the red, green and blue structures integrated in the RGB pixel operate independently.

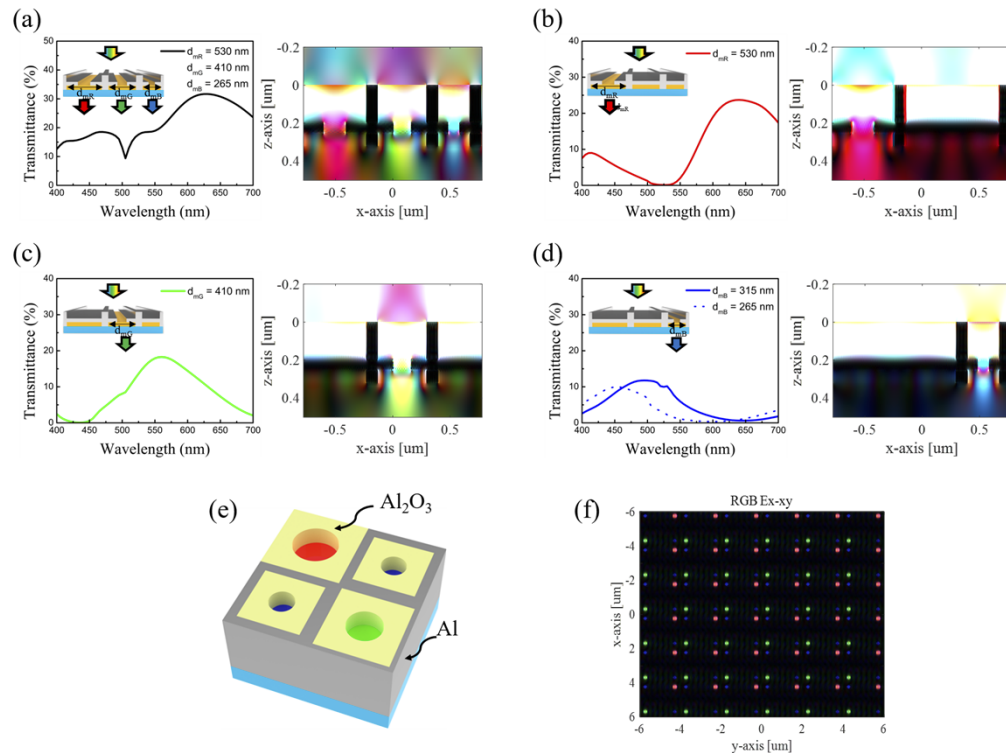


Fig. 7. Optical characteristics of RGB pixel structure with integrated 1D single pixel PCF that transmits red, green, and blue. The individual switching structures of (a) white, (b) red, (c) green and (d) blue color filtering mode. Distance between metallic mirror sidewalls results in 315 nm (solid line), 265 nm (dashed line). RGB pixel structure with integrated 2D single pixel color filter. (e) Schematic of RGB composite single hole color filter. (f) Electric field color visualization of the RGB and white color filtering modes.

Next, the independently operating color filter properties of the red, green and blue structures were analyzed. For example, block the metal slits in the green and blue positions to see the independent operation of the red structure. Figure 7(b) present the numerical result of the independent red pixel with a transmittance of 23.7% at 640 nm and a FWHM of 147.5 nm.

The image visualized electric field distribution generated when electromagnetic waves of 633 nm, 532 nm and 473 nm wavelengths are incident on the structure shows that the transmitted beam electric field is dominated by a red light of 633 nm. In Figs. 7(c) and 7(d), the green structure shows a resonance wavelength of 560 nm, transmittance of 18.3%, and FWHM of 136.5 nm, and in Fig. 7(d), the blue structure shows a resonance wavelength of 495 nm, transmittance of 11.8%, and FWHM of 117.5 nm. In Fig. 7(d), the resonance wavelength is red shifted and a transmittance peak is formed at 495 nm, that is, the pure blue color is not transmitted. The variable distance between metallic mirror sidewalls, which is an effective parameter for shifting

the resonance wavelength, can induce a shift from 495 nm to 455 nm. Figure 7(e) presents a design for a 2D RGB composite color pixel. Red, green and two blue filters are compactly integrated into a rectangular area with lateral dimensions of $1.1 \mu\text{m} \times 1.1 \mu\text{m}$. The transmitted electric field distribution of the composite color pixel under white light is visualized in Fig. 7(f), proving that all color filters clearly operate without inter-pixel crosstalk. In these example designs, the distance between each unit color filters are chosen longer than 80 nm to ensure completely independent color pixel operation, but we expect that the dimension of the RGB composite color pixel can be reduced to the submicron scale using a more compact design employing more PEC like materials. We expect to make progress in that area as our next research topic.

4. Conclusion

In conclusion, we have presented a PCF full-color HD-CGH concept. From a comparative analysis with a conventional HD-CGH with an additional color filter layer, we have argued that the proposed in-plane color pixel can develop HD-CGH coloration technology. The design of a $1.505 \mu\text{m} \times 1.505 \mu\text{m}$ RGB 1D PCF and $1.1 \mu\text{m} \times 1.1 \mu\text{m}$ RBGB 2D PCF composite single pixel for HD-CGH has been derived. We have verified the aperiodic single unit operation of the proposed color pixel structure with an analysis of its transmission spectrum, color gamut, and incident angle dependence, and we proposed the design of single pixel PCF based wide-viewing full-color HD CGHs.

Appendix I: Periodic color filter structures

The 1D and 2D periodic PCFs are the basis for designing the single pixel PCF. In Fig. 8, both structures are made of metal and dielectric materials with a high refractive index, and plasmonic resonances at red, green, and blue wavelengths are induced inside the structures with specific values of period, fill factor and layer thickness.

The 1D grating structure in Fig. 8(a) consists of a 65 nm dielectric (ZrO_2) layer and a 55 nm metal (Al) grating on a quartz substrate. In this structure, the dielectric layer acts as a waveguide, and the incident waves are diffracted by the metal grating and generates constructive resonance with the resonant waveguide mode. This leads to resonant optical transmission of the desired wavelength being observed. The grating periods, Λ_g for the red, green and blue 1D color filter are 530 nm, 410 nm, 315 nm, respectively, and the fill factor is the same 0.65 for all colors. As shown in Fig. 8(c), when TM polarized incident light enters, the periodic grating structure transmits red, green and blue light with transmittances of 75%, 76%, and 68%, respectively. In the single slit structure, where the periodicity has disappeared, the waveguide mode is not excited because the grating vector does not exist. Therefore, the light is transmitted evenly in the visible region following the plot indicated by the dashed line, and there is no filter function. Fig. 8(b) presents the 2D periodic hole patterned structure that consists of a 200 nm thick dielectric (Al_2O_3) layer and a 150 nm thick metal (Al) hole pattern on a quartz substrate. A square-lattice hole array is patterned on the aluminum layer for the excitation of surface plasmon resonance, and the dielectric layer is deposited on it for enhanced color purity. The periods Λ_h corresponding to the red, green, and blue colors are 420 nm, 370 nm and 320 nm, respectively, and the hole diameter is 240 nm, 180 nm, and 130 nm. As shown in Fig. 8(d), when TM or TE polarized light is normally incident on the hole pattern structure, the transmittance of the red, green, and blue colors are 10%, 10%, and 9%, respectively. Similar to the 1D slit transmission, an aperiodic single hole unit transmits light evenly over the visible wavelength band without band-pass filtering features on specific wavelength. As manifested in the main section, periodicity can be a major hindrance when attempting to spatially integrate color filters across a wide range of novel photonics applications. The HD-CGH is one of those applications that require highly compact single pixel PCFs.

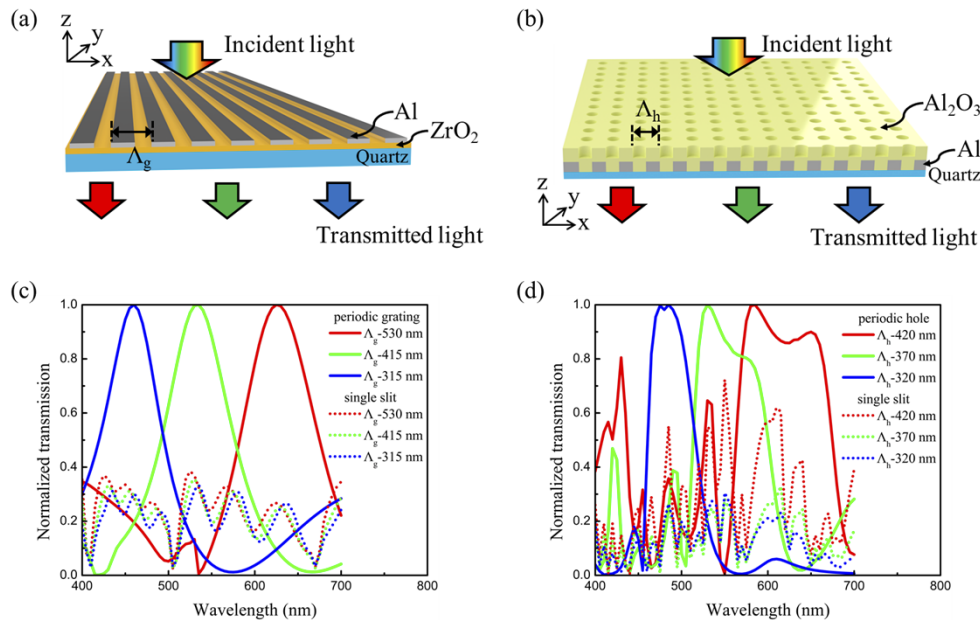


Fig. 8. Schematic and optical properties of PCF structures made of dielectric and metal. Schematic of periodic (a) 1D grating and (b) 2D hole pattern structures. (c, d) Calculated transmission spectrum of designed R/G/B color filters depend on presence of periodicity. (c) The 1D structure transmittance spectrum is represented by colors with different Λ_g (530 nm, 410 nm and 315 nm). (d) The 2D structure transmittance spectrum is represented by colors with different Λ_h (420 nm, 370 nm and 320 nm). The solid line indicates the spectrum of the periodic structure and the dashed line indicates that of non-periodic single unit structure.

Appendix II: PEC single pixel color filter

Even when designing a metallic color filter using real metals, it would be valuable to understand a single pixel color filter made of perfect electric conductor (PEC) mirror sidewall. In Fig. 9(a), the PEC mirror sidewall is erected vertically from the substrate, and its shape is determined by the height h_m and width w_m .

The PEC mirror sidewalls are placed on both sides of a single slit to form a Fabry-Pérot nanocavity. Fig. 9(b) shows that the PEC mirror sidewalls are placed on both sides of a single slit to form a nanocavity and a Fabry-Pérot interferometer is formed. Standing waves are formed inside the dielectric layer and an electric field of strong intensity is transmitted. As shown in Fig. 9(c), the transmittance of the red structure is 21.6% at 605 nm, the green structure is 19.4% at 530 nm, and the blue structure is 13.3% at 475 nm. These results with PEC sidewalls reveal an efficiency approximately 5% higher than with the real metallic mirror sidewalls.

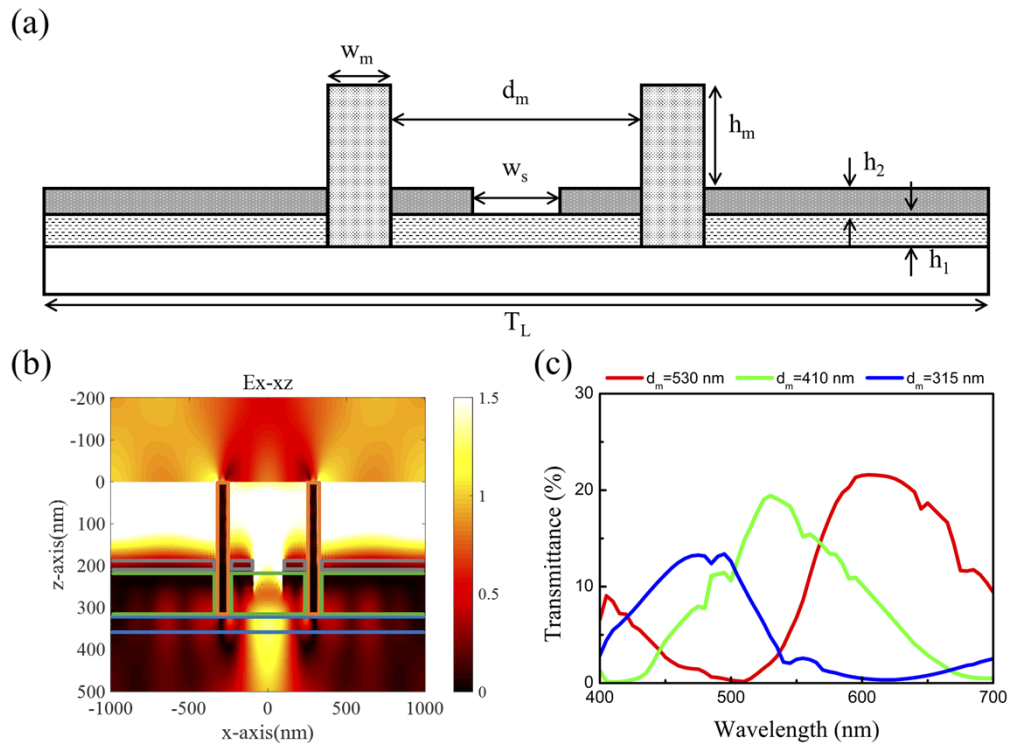


Fig. 9. Single pixel PCF with PEC mirror sidewall. (a) Schematic illustration of the single pixel PCF structure. Schematic illustration of the single pixel PCF structure. Representative red color structure parameters are 530 nm of d_m , 344.5 nm of w_s , 200 nm of h_m , 65 nm of h_1 , and 55 nm of h_2 . (b) Electric field distribution profile in x - z cross-section of 1D single pixel PCF. (Observed in red color structure at 633 nm wavelength). (c) Calculated red, green, and blue structure transmittance spectrum of 1D structures. d_m is the distance between the PEC mirror sidewalls. The d_m corresponding to the red, green and blue structures are 530 nm, 410 nm, and 315 nm, respectively.

Appendix III: Optical characteristics of single pixel PCF

We analyze the optical properties that change with mirror wall width to consider the effect of the mirror sidewall width of a single pixel PCF. In Fig. 10(a), the variables of the single pixel PCF structure are defined by w_m (mirror width), d_m (mirror distance), w_s (slit width), T_L (length along the x -axis), h_1 (dielectric layer height), h_2 (metal layer thickness) and h_m (mirror height). d_m , w_m , w_s , T_L , h_1 , h_2 , and h_m are 530 nm, 50 nm, 344.5 nm, 2 μm , 65 nm, 55 nm, 200 nm, respectively, for the red color filter, 410 nm, 50 nm, 266.5 nm, 2 μm , 65 nm, 55 nm, 200 nm, respectively, for the green colors, and 315 nm, 204.75 nm, 2 μm , 65 nm, 55 nm and 200 nm for the blue color, respectively.

At first, the red color filter is considered. Fig. 10(b) plots an analysis of the optical properties occurring in the range from no mirror sidewall (0 nm) to a mirror sidewall of 600 nm width w_m . The structure with no metallic mirror sidewall does not induce resonance, and a 40 nm (w_m) metallic mirror sidewall has a resonance wavelength of 630 nm, a transmittance of 15.9%, and a FWHM of 137.5 nm. At w_m of 80 nm, a dip occurs at 665 nm and a secondary peak occurs at 670 nm. In Fig. 10(b), this secondary peak becomes a single peak at 120 nm w_m and shifts to a long wavelength to become a resonator at 670 nm. The peak generated at 670 nm is maintained up to the w_m of 300 nm and operates as a red color filter, but over w_m of 300 nm, the intensity of

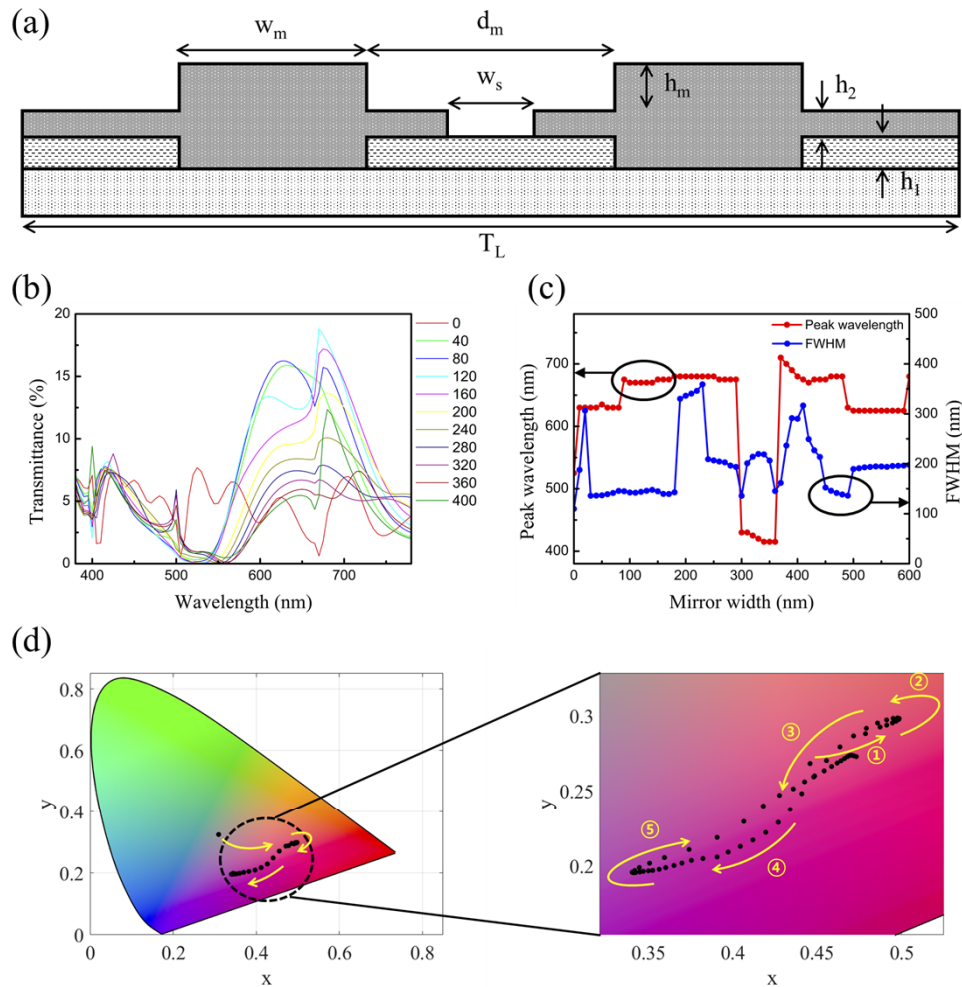


Fig. 10. Optical properties of 1D red ($d_m = 530$ nm) color single pixel PCF dependent on metallic sidewall width. (a) Schematic illustration of the single pixel PCF structure. Representative red color structure parameters are a 530 nm d_m , 344.5 nm w_s , 200 nm h_m , 65 nm h_1 , and 55 nm h_2 . (b) Transmittance spectrum for w_m ranging from 0 nm to 400 nm. (c) Calculated peak wavelength and FWHM for the variable w_m (solid red line is peak wavelength and blue solid line is FWHM). (d) CIE 1931 color diagram with calculated color coordinates according to w_m in the range from 0 nm to 600 nm.

the first order peak decreases, and a range lower than the intensity of the sidelobe of 420 nm is observed in Fig. 10(c). The first order peak decrease from 300 nm to 360 nm of w_m is to be avoided in the structure for transmitting red color. The unstable peak wavelength and FWHM below 20 nm are judged to be affected by the penetration depth of Al, the material used in the simulation [29]. The results observed while varying w_m are expressed in the color coordinate system, and the representatively calculated red single pixel PCF color implementation is shown in Fig. 10(d). The 0 nm w_m without a metallic mirror sidewall is located in the center of the color coordinate system and is red-shifted by the metallic mirror sidewall. The color purity of red is high at w_m values below 100 nm, and a blue shift is observed as it increases from 110 nm to 400 nm.

As shown in Fig. 11(a), for the green structure, the transmittance spectrum changes according to the metallic mirror sidewall and exhibits maximum efficiency at a w_m of 40 nm, gradually decreasing at higher w_m to saturate at approximately 10%. In Fig. 11(b), the peak wavelength has an average value of 554.5 nm in the w_m range from 0 nm to 600 nm, and the FWHM has an average value of 123 nm. Overall, the green structure shows low w_m dependence in terms of transmittance spectrum. As shown in Fig. 11(c), the changes in optical properties with w_m can be considered within the CIE color coordinate system. As w_m increases from 10 nm to 300 nm, the color shifts to the green region and color purity gradually increases. The highest color purity is apparent from 310 nm to 350 nm.

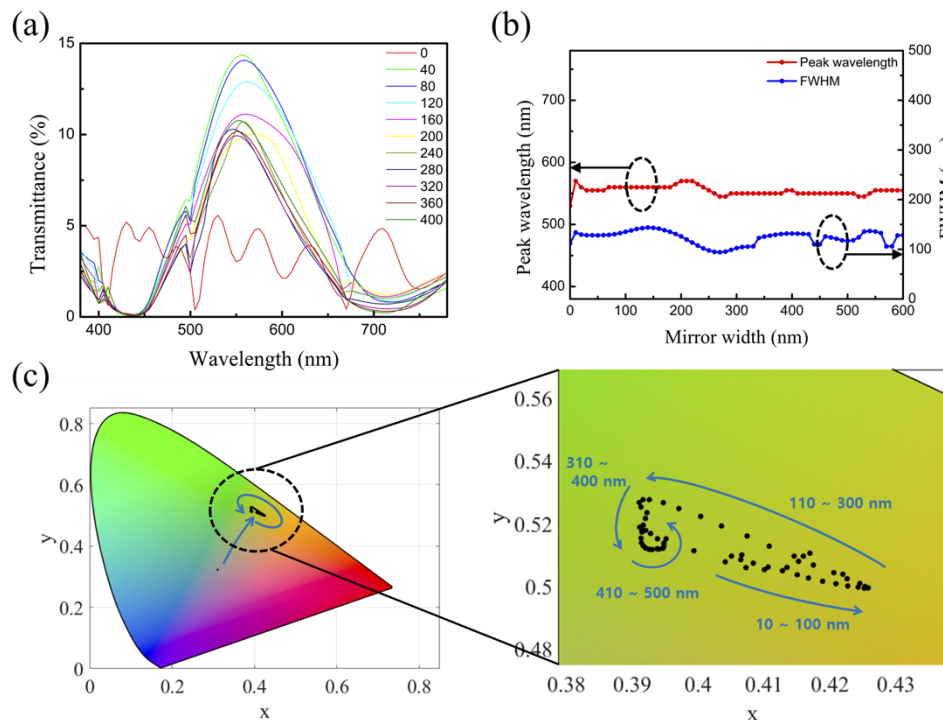


Fig. 11. Green color single pixel PCF according to variable w_m . (a) Transmittance spectrum with w_m ranging from 0 nm to 400 nm. (b) Peak wavelength and FWHM expressed within the variable range of w_m . Solid red line is peak wavelength and blue solid line is FWHM. (c) CIE 1931 color diagram with calculated color coordinates according to w_m in the range from 0 nm to 600 nm.

In Fig. 12(a), the transmittance spectrum of the blue structure shows transmittance within the maximum range of 10% and minimum of 8% as w_m increases. A noteworthy point in the blue

structure is that a dip exists at the wavelength of 500 nm, and the peak existing at a wavelength lower than the dip becomes a first order peak and approaches pure blue color. The dip observed in the transmittance spectrum causes two peaks to coexist so that the peak wavelength changes depending on the conditions. As shown in Fig. 12(b), in the w_m range from 30 nm to 110 nm, a wavelength peak is formed at 515 nm on average, whereas in the range from 120 nm to 390 nm, a wavelength peak is formed at 475 nm on average, which means that, in terms of expressing blue color, a w_m from 120 nm to 390 nm is more suitable. Furthermore, as w_m increases from 10 nm to 360 nm, it gradually approaches the blue region, but then shifts towards the green region as w_m exceeds 310 nm. Since it has significantly shifted to the green region, a w_m of 360 nm is the optimal condition for blue color expression.

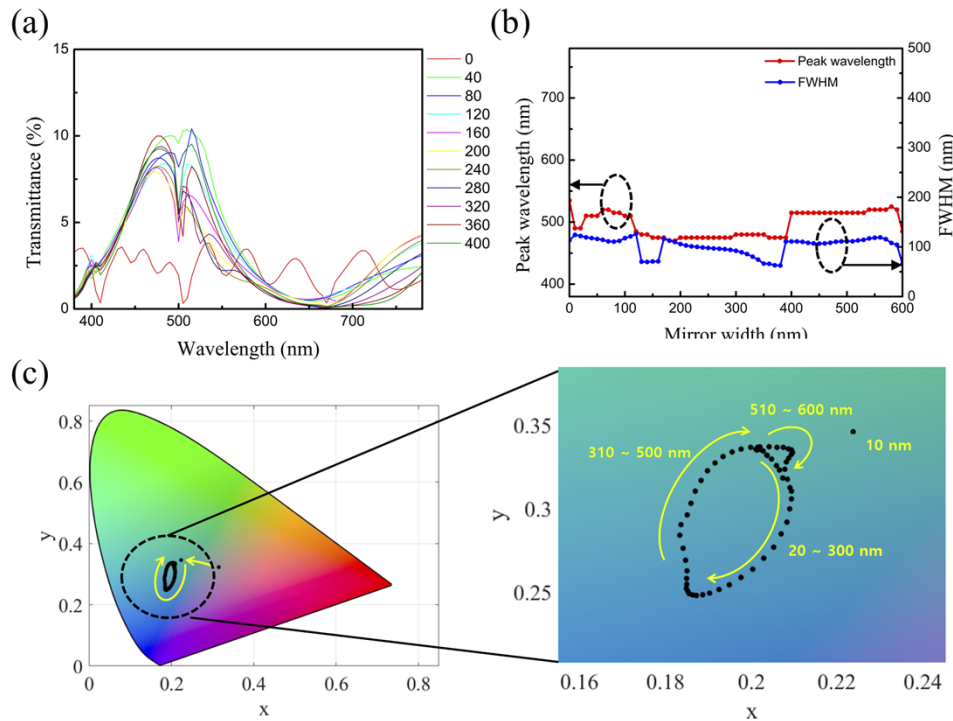


Fig. 12. Blue color single pixel PCF according to variable w_m . (a) Transmittance spectrum with w_m ranging from 0 nm to 400 nm. (b) Peak wavelength and FWHM expressed within the variable range of w_m . Solid red line is peak wavelength and blue solid line is FWHM. (c) CIE 1931 color diagram with calculated color coordinates according to w_m in the range from 0 nm to 600 nm.

Funding. Institute of Information & Communications Technology Planning & Evaluation (IITP) (No. 2020-0-00914).

Disclosures. The authors declare no conflicts of interest.

Data availability. Data underlying the results presented in this paper are not publicly available at this time but may be obtained from the authors upon reasonable request.

References

1. C. Genet and T. W. Ebbesen, "Light in tiny holes," *Nature* **445**(7123), 39–46 (2007).
2. G. Si, Y. Zhao, J. Lv, M. Lu, F. Wang, H. Liu, N. Xiang, T. J. Huang, A. J. Danner, and J. Teng, "Reflective plasmonic color filters based on lithographically patterned silver nanorod arrays," *Nanoscale* **5**(14), 6243–6248 (2013).
3. Y. S. Do, J. H. Park, B. Y. Hwang, S. M. Lee, B. K. Ju, and K. C. Choi, "Plasmonic color filter and its fabrication for large-area applications," *Adv. Opt. Mater.* **1**(2), 133–138 (2013).

4. Y. Zhao, Y. Zhao, S. Hu, J. Lv, Y. Ying, G. Gervinskias, and G. Si, "Artificial structural color pixels: A review," *Materials* **10**(8), 944 (2017).
5. W. Tian and J. Li, "Size- dependent optical-electrical characteristics of blue GaN/InGaN micro-light-emitting diodes," *Appl. Opt.* **59**(29), 9225–9232 (2020).
6. Y. Guo, H. Shahsavani, and M. Sitti, "Microscale polarization color pixels from liquid crystal elastomers," *Adv. Opt. Mater.* **8**(17), 1902098 (2020).
7. Q. Chen and D. R. Cumming, "High transmission and low color cross-talk plasmonic color filters using triangular-lattice hole arrays in aluminum films," *Opt. Express* **18**(13), 14056–14062 (2010).
8. D. Fleischman, L. A. Sweatlock, H. Murakami, and H. Atwater, "Hyper-selective plasmonic color filters," *Opt. Express* **25**(22), 27386–27395 (2017).
9. A. Ghobadi, H. Hajian, M. C. Soydan, B. Butun, and E. Ozbay, "Lithography-free planar band-pass reflective color filter using a series connection of cavities," *Sci. Rep.* **9**(1), 290 (2019).
10. Y. Gu, L. Zhang, J. K. Yang, S. P. Yeo, and C. W. Qiu, "Color generation via subwavelength plasmonic nanostructures," *Nanoscale* **7**(15), 6409–6419 (2015).
11. D. Inoue, A. Miura, T. Nomura, H. Fujikawa, K. Sato, N. Ikeda, D. Tsuya, Y. Sugimoto, and Y. Koide, "Polarization independent visible color filter comprising an aluminum film with surface-plasmon enhanced transmission through a subwavelength array of holes," *Appl. Phys. Lett.* **98**(9), 093113 (2011).
12. K. T. Lee, S. Y. Han, Z. Li, H. W. Baac, and H. J. Park, "Flexible high-color-purity structural color filters based on a higher-order optical resonance suppression," *Sci. Rep.* **9**(1), 14917 (2019).
13. J. Wang, Q. Fan, S. Zhang, Z. Zhang, H. Zhang, Y. Liang, X. Cao, and T. Xu, "Ultra-thin plasmonic color filters incorporating free-standing resonant membrane waveguides with high transmission efficiency," *Appl. Phys. Lett.* **110**(3), 031110 (2017).
14. C. Yang, W. Shen, Y. Zhang, K. Li, X. Fang, X. Zhang, and X. Liu, "Compact multilayer film structure for angle insensitive color filtering," *Sci. Rep.* **5**(1), 9285 (2015).
15. E. H. Cho, H. S. Kim, B. H. Cheong, P. Oleg, W. Xianyu, J. S. Sohn, D. J. Ma, H. Y. Choi, N. C. Park, and Y. P. Park, "Two-dimensional photonic crystal color filter development," *Opt. Express* **17**(10), 8621–8629 (2009).
16. A. F. Kaplan, T. Xu, Y. K. Wu, and L. J. Guo, "Multilayer pattern transfer for plasmonic color filter applications," *J. Vac. Sci. Technol., B: Nanotechnol. Microelectron.: Mater., Process., Meas., Phenom.* **28**(6), C6O60–C6O63 (2010).
17. F. J. Ko and H. P. D. Shieh, "High-efficiency micro-optical color filter for liquid-crystal projection system applications," *Appl. Opt.* **39**(7), 1159–1163 (2000).
18. S. U. Lee and B. K. Ju, "Wide-gamut plasmonic color filters using a complementary design method," *Sci. Rep.* **7**(1), 1–5 (2017).
19. V. R. Shrestha, C. S. Park, and S. S. Lee, "Enhancement of color saturation and color gamut enabled by a dual-band color filter exhibiting an adjustable spectral response," *Opt. Express* **22**(3), 3691–3704 (2014).
20. Y. Wang, M. Zheng, Q. Ruan, Y. Zhou, Y. Chen, P. Dai, Z. Yang, Z. Lin, Y. Long, and Y. Li, "Stepwise-nanocavity-assisted transmissive color filter array microprints," *Research* **2018**, 1–10 (2018).
21. S. P. Burgos, S. Yokogawa, and H. A. Atwater, "Color imaging via nearest neighbor hole coupling in plasmonic color filters integrated onto a complementary metal-oxide semiconductor image sensor," *ACS Nano* **7**(11), 10038–10047 (2013).
22. Q. Chen, D. Chitnis, K. Walls, T. D. Drysdale, S. Collins, and D. R. Cumming, "CMOS photodetectors integrated with plasmonic color filters," *IEEE Photonics Technol. Lett.* **24**(3), 197–199 (2012).
23. Y. Liu, G. Si, E. Leong, B. Wang, A. Danner, X. Yuan, and J. Teng, "Optically tunable plasmonic color filters," *Appl. Phys. A* **107**(1), 49–54 (2012).
24. A. Miyamichi, A. Ono, K. Kagawa, K. Yasutomi, and S. Kawahito, "Plasmonic color filter array with high color purity for CMOS image sensors," *Sensors* **19**(8), 1750 (2019).
25. T. Xu, Y. K. Wu, X. Luo, and L. J. Guo, "Plasmonic nanoresonators for high-resolution colour filtering and spectral imaging," *Nat. Commun.* **1**(1), 59 (2010).
26. D. Fleischman, K. T. Fountaine, C. R. Bukowsky, G. Tagliabue, L. A. Sweatlock, and H. A. Atwater, "High spectral resolution plasmonic color filters with subwavelength dimensions," *ACS Photonics* **6**(2), 332–338 (2019).
27. H. Yun, S. Y. Lee, K. Hong, J. Yeom, and B. Lee, "Plasmonic cavity-apertures as dynamic pixels for the simultaneous control of colour and intensity," *Nat. Commun.* **6**(1), 7133 (2015).
28. J. K. Hyun, T. Kang, H. Baek, D. S. Kim, and G. C. Yi, "Nanoscale single-element color filters," *Nano Lett.* **15**(9), 5938–5943 (2015).
29. V. J. Sorger, R. F. Oulton, J. Yao, G. Bartal, and X. Zhang, "Plasmonic Fabry-Pérot nanocavity," *Nano Lett.* **9**(10), 3489–3493 (2009).
30. S. Park, J. Lee, S. Lim, M. Kim, S. Ahn, S. Hwang, S. Jeon, J. Jeong, J. Hahn, and H. Kim, "Wide-viewing full-color depthmap computer-generated holograms," *Opt. Express* **29**(17), 26793–26807 (2021).
31. O. Kunieda and K. Matsushima, "High-quality full-parallax full-color three-dimensional image reconstructed by stacking large-scale computer-generated volume holograms," *Appl. Opt.* **58**(34), G104–G111 (2019).
32. K. Matsushima and N. Sonobe, "Full-color digitized holography for large-scale holographic 3D imaging of physical and nonphysical objects," *Appl. Opt.* **57**(1), A150–A156 (2018).
33. Y. Tsuchiyama and K. Matsushima, "Full-color large-scaled computer-generated holograms using RGB color filters," *Opt. Express* **25**(3), 2016–2030 (2017).

34. C. Y. Hwang, G. H. Kim, J. H. Yang, C. S. Hwang, S. M. Cho, W. J. Lee, J. E. Pi, J. H. Choi, K. Choi, H. O. Kim, S. Y. Lee, and Y. H. Kim, "Rewritable full-color computer-generated holograms based on color-selective diffractive optical components including phase-change materials (vol 10, pg 21648, 2018)," *Nanoscale* **10**(47), 22635 (2018).
35. H. Kim, J. Park, and B. Lee, *Fourier Modal Method and Its Applications in Computational Nanophotonics* (CRC, 2012).
36. D. Felbacq, A. Moreau, and R. Smaïli, "Goos-Hänchen effect in the gaps of photonic crystals," *Opt. Lett.* **28**(18), 1633–1635 (2003).
37. Y. P. Wong, Y. Miao, J. Skarda, and O. Solgaard, "Large negative and positive optical Goos-Hänchen shift in photonic crystals," *Opt. Lett.* **43**(12), 2803–2806 (2018).
38. F. Behroozi and M. Garfunkel, "Penetration depth in superconducting aluminum as a function of magnetic field and temperature," *Physica* **55**, 649–655 (1971).